

The contribution of high redshift galaxies to the Near-Infrared Background

Bin Yue^{1,3,5}, Andrea Ferrara^{1,6}, Ruben Salvaterra², Xuelei Chen^{3,4}

ABSTRACT

Several independent measurements have confirmed the existence of fluctuations ($\delta F_{\text{obs}} \approx 0.1 \text{ nW/m}^2/\text{sr}$ at $3.6 \mu\text{m}$) up to degree angular scales in the source-subtracted Near InfraRed Background (NIRB) whose origin is unknown. By combining high resolution cosmological N-body/hydrodynamical simulations with an analytical model, and by matching galaxy Luminosity Functions (LFs) and the constraints on reionization simultaneously, we predict the NIRB absolute flux and fluctuation amplitude produced by high- z ($z > 5$) galaxies (some of which harboring Pop III stars, shown to provide a negligible contribution). This strategy also allows us to make an empirical determination of the evolution of ionizing photon escape fraction: we find $f_{\text{esc}} = 1$ at $z \geq 11$, decreasing to ≈ 0.05 at $z = 5$. In the wavelength range $1.0 - 4.5 \mu\text{m}$, the predicted cumulative flux is $F = 0.2 - 0.04 \text{ nW/m}^2/\text{sr}$. However, we find that the radiation from high- z galaxies (including those undetected by current surveys) is insufficient to explain the amplitude of the observed fluctuations: at $l = 2000$, the fluctuation level due to $z > 5$ galaxies is $\delta F = 0.01 - 0.002 \text{ nW/m}^2/\text{sr}$, with a relative wavelength-independent amplitude $\delta F/F = 4\%$. The source of the missing power remains unknown. This might indicate that an unknown component/foreground, with a clustering signal very similar to that of high- z galaxies, dominates the source-subtracted NIRB fluctuation signal.

osmology: diffuse radiation–galaxies: high redshift–methods: numerical.

1. INTRODUCTION

Observations of high redshift galaxies are essential to understand cosmic reionization. Although current surveys have reached redshifts $\sim 8 - 10$ (Bouwens et al. 2010, 2011a,b), it is generally believed that the sources detected so far, usually rare and bright galaxies, are not the dominant

¹Scuola Normale Superiore, Piazza dei Cavalieri 7, I-56126 Pisa, Italy

²INAF, IASF Milano, via E. Bassini 15, I-20133 Milano, Italy

³National Astronomical Observatories, Chinese Academy of Sciences, 20A Datun Road, Chaoyang, Beijing 100012, China

⁴Center of High Energy Physics, Peking University, Beijing 100871, China

⁵Graduate University of Chinese Academy of Sciences, Beijing 100049, China

⁶Centennial B. Tinsley Professor, University of Texas, Austin, USA

contributors to reionization (Choudhury & Ferrara 2007; Lorenzoni et al. 2011; Jaacks et al. 2012; Finkelstein et al. 2012). Instead, reionization is likely powered by the large number of galaxies that are still below the detection limit.

Even without detecting these faint galaxies individually, their cumulative radiations may still tell us much about their properties. Indeed, the bulk of their emission, mostly in the band between the Lyman limit and the visible light, is redshifted into the near InfraRed (IR) at present time. Therefore, the Near InfraRed Background (NIRB) which is obtained after removing the contributions from the Solar system, the Milky Way and low- z galaxies, could provide a wealth of information on high redshift galaxies, such as their integrated emissivity and large scale clustering properties.

The NIRB measurement has a history dating back to more than two decades (see the review by Kashlinsky 2005). Early measurements gave a NIRB flux $\gtrsim 10$ nW/m²/sr (Dwek & Arendt 1998; Gorjian et al. 2000; Matsumoto et al. 2000; Cambr esy et al. 2001; Matsumoto et al. 2005). These works showed that a non-zero residual remains after the foreground and the emission from known galaxies are removed (Totani et al. 2001; Matsumoto et al. 2005). Salvaterra & Ferrara (2003) and Santos et al. (2002) suggested that Pop III stars could possibly be the sources of such leftover signal. If true, this residual would be an exquisite tool to study Pop III stars. However, not long afterwards, Madau & Silk (2005) and Salvaterra & Ferrara (2006) found that this scenario needs a very high star formation efficiency and may overpredict the high- z dropouts galaxies¹. To solve this problem, we need either an alternative theoretical explanation (proved hard to be found), or a more accurate determination of the residual flux, or both.

Due to the difficulties in foreground subtraction (Dwek et al. 2005), in recent observational works more attentions are paid to the angular fluctuations. In such observations, the influence of strong but smooth foregrounds, such as the zodiacal light, is reduced, and one can also infer the large scale clustering properties of the unknown sources (Kashlinsky et al. 2002, 2004; Magliocchetti et al. 2003; Cooray et al. 2004; Matsumoto et al. 2005; Salvaterra et al. 2006). The recent measurements (Kashlinsky et al. 2005, 2007a, 2012; Matsumoto et al. 2005, 2011; Thompson et al. 2007a,b; Cooray et al. 2012b) have obtained angular power spectra of the source-subtracted NIRB (i.e. all resolved galaxies have been removed) at wavelengths from 1.1 μ m to 8 μ m. These angular power spectrum measurements show that the sources have a large clustering signal up to degree scales.

The source-subtracted NIRB fluctuations are found to be much higher than the theoretically predicted contribution from low- z faint galaxies. Although Kashlinsky et al. (2005, 2007b); Matsumoto et al. (2011); Kashlinsky et al. (2012) favored a scenario in which the observed fluctuations come from Pop III stars, Cooray et al. (2012a) showed that, to be consistent with the electron

¹A significant contribution from high- z mini-quasars powered by accretion on to intermediate mass black holes with spectra similar to local Ultra-Luminous X-ray sources is disfavored on the basis of the unresolved X-ray background intensity constraints (Salvaterra et al. 2005), unless these objects are highly absorbed by the surrounding gas.

scattering optical depth measured by WMAP (Komatsu et al. 2011), the contribution from high- z galaxies (including Pop III stars) must be smaller by at least an order of magnitude than what is observed. Instead, Cooray et al. (2012b) suggested recently that a large fraction of the observed NIRB fluctuations comes from the diffuse light of intrahalo stars at intermediate redshifts ($z \sim 1$ to 4). While an intriguing idea, this explanation relies on the poorly known fraction and spectral energy distribution of intrahalo stars. It also predicts, contrary to the faint distant galaxies hypothesis, that fluctuations induced by the much closer intrahalo stars should extend into the optical bands, where the light from first galaxies is blanketed by intervening intergalactic neutral hydrogen. Numerical simulations by Fernandez et al. (2010, 2012) stressed the importance of nonlinear effects in theoretical calculations as a possible way to reconcile the theory with data.

There have also been proposals that the sources of these fluctuations are lower redshift galaxies (Thompson et al. 2007b; Cooray et al. 2007; Chary et al. 2008), but this possibility has become less attractive by now. Indeed, Helgason et al. (2012) recently reconstructed the emissivity history from the luminosity functions (LFs) of observed galaxies, and found that the fluctuations from the known galaxy population below the detection limit are unable to account for the observed clustering signal on sub-degree angular scales.

To make further progress, it is essential to make more accurate predictions of the NIRB contributed by Pop III stars and the galaxies before reionization, using models which are consistent with *all* current observational constraints, including both the high redshift LFs and reionization.

In this paper, we attempt to make the most detailed theoretical NIRB model developed so far, with predictions on both the absolute flux and the angular power spectrum contributed by high- z galaxies. To do this, we used a simulation with detailed treatment of the relevant physics of star/galaxy formation, including gas dynamics, radiative cooling, supernova explosion, photoionization and heating, and especially a detailed treatment of chemical feedback (Tornatore et al. 2007a,b). The LFs of high redshift galaxies in the simulation match remarkably well with observations, this is the starting point of our NIRB model.

The layout of the paper is as follows. In Section 2 we introduce the simulation, and describe the steps to calculate the NIRB absolute flux and the angular power spectrum. In Section 3 we present our results and compare them with observations. Conclusions are presented in Section 4. In Appendix A we compare the different approximate solutions for the analytical calculation of the emissivity. Throughout this paper, we use the same cosmological parameters as in Salvaterra et al. (2011): $\Omega_m=0.26$, $\Omega_\Lambda=0.74$, $h=0.73$, $\Omega_b=0.041$, $n = 1$ and $\sigma_8=0.8$. The transfer function is from Eisenstein & Hu (1998). Magnitudes are given in the AB system.

2. METHOD

2.1. The Absolute Flux

At $z = 0$, the cumulative flux of the NIRB observed at frequency ν_0 is the integrated contribution of sources whose emission is shifted into a band of central frequency ν_0 . Following Salvaterra et al. (2006), we write it as

$$\begin{aligned}
 F &= \nu_0 I_{\nu_0} \\
 &= \nu_0 \int_{z_{\min}}^{z_{\max}} \epsilon(\nu, z) e^{-\tau_{\text{eff}}(\nu_0, z)} \frac{dr_p}{dz} dz \\
 &= \int_{z_{\min}}^{z_{\max}} cdz \frac{\nu \epsilon(\nu, z) e^{-\tau_{\text{eff}}(\nu_0, z)}}{H(z)(1+z)^2}, \tag{1}
 \end{aligned}$$

where r_p is the proper distance, $\nu = (1+z)\nu_0$ is the rest frame frequency, $\epsilon(\nu, z)$ is the comoving specific emissivity, $H(z)$ is the Hubble parameter given by $H(z) = H_0 \sqrt{\Omega_m(1+z)^3 + \Omega_\Lambda}$ in a flat Λ CDM cosmology, c is the speed of light. The effective optical depth of absorbers between redshift 0 and z , τ_{eff} , is composed of two parts: the line absorption and the continuum absorption; we use the expressions in Salvaterra & Ferrara (2003).

We calculate the emissivity (see also Appendix for further discussions on subtleties related to the various approximations used in the literature) from the results of the simulation presented in Salvaterra et al. (2011), which includes a detailed treatment of chemical enrichment developed by Tornatore et al. (2007a). In our model, both Pop II stars and Pop III stars are assumed to follow the Salpeter initial mass function (IMF) (Salpeter 1955), for Pop II stars the mass range is $0.1 - 100 M_\odot$, while for Pop III stars the mass range is set to be $100 - 500 M_\odot$. Some recent works indicate that Pop III stars may not be so massive as was predicted previously, but may be limited to $\lesssim 50 M_\odot$ (Hosokawa et al. 2011). Our choice then corresponds to an upper limit to the contribution of these sources. Using this simulation, Salvaterra et al. (2011) generated the LFs of galaxies down to the magnitude far below the current observation limits at high redshifts. In the redshift range $5 < z < 10$, the simulated LFs match the observed ones almost perfectly in the overlapping luminosity range.

Suppose the specific luminosity of the i -th galaxy in the simulation box is $L_\nu^i(z)$ at redshift z ,

the comoving specific emissivity is then ²

$$\epsilon(\nu, z) = \frac{1}{4\pi} \frac{\sum_{i=1}^N L_{\nu}^i(z)}{V}, \quad (2)$$

where V is the comoving volume of the simulation, N is the total number of galaxies in the simulation box at redshift z .

In the emissivity calculation, we must correct for rare bright galaxies that are not caught by the simulation due to the finite box size ($10 h^{-1}\text{Mpc}$). We follow the steps in Salvaterra et al. (2011). We first calculate the absolute magnitude corresponding to the mean luminosity of the two brightest galaxies in the simulation box, $M_{\text{UV,up}}$. The contribution (to be added to the numerator in Eq. (2)) from galaxies brighter than this magnitude is obtained by integration

$$L_{\nu}^{\text{corr}}(z) = V \int_{-25}^{M_{\text{UV,up}}} L_{\nu}^1(z) \frac{L_{\text{UV}}}{L_{\nu_{\text{UV}}}^1(z)} \Phi(M_{\text{UV}}, z) dM_{\text{UV}}, \quad (3)$$

where $L_{\nu}^1(z)$ is the luminosity of the brightest galaxy in the simulation (we assume all rare bright galaxies have the same Spectral Energy Distribution (SED) of this one), L_{UV} is the luminosity corresponding to the UV absolute magnitude M_{UV} . The wavelength used to calculate the absolute UV magnitude in this paper is 1700 \AA , ν_{UV} is the frequency corresponding to this wavelength. In observations, the selected wavelength corresponding to the UV absolute magnitude may be somewhat different in different measurements and at different redshifts (Bouwens et al. 2007; Oesch et al. 2010; Bouwens et al. 2010), however, our results are not sensitive to such differences. For the LF $\Phi(M_{\text{UV}}, z)$ in the redshift range $5 < z < 10$, we use the Schechter formula (Schechter 1976) with the redshift-dependent parameters given by Bouwens et al. (2011b) (see their Sec. 7.5), who fitted the observed LFs in $z \sim 4 - 8$ and extrapolated them to higher redshifts. For redshifts above 10, we simply add an exponential tail normalized to the simulated LF amplitude at $M_{\text{UV,up}}$. We find that this results only a small correction. As discussed below (see also bottom panel of Figure 3), $\sim 90\%$ of the high- z galaxy contribution to the NIRB flux comes from sources at $5 < z < 8$ where the correction is at most 12%. This correction is also applied to the calculation of ionizing photons below.

For each galaxy, the radiation comes from two different mechanisms: the stellar emission and the nebular emission. The former comes directly from the surface of stars, while the latter is generated by the ionized nebula around stars and depends on the fraction of ionizing photons

²The dust absorption in the host galaxy may lower its luminosity in the rest frame UV band, therefore reduce their contribution to the NIRB. However, as shown by Salvaterra et al. (2011), for high redshift dwarf galaxies considered by us here, this effect is negligible. The absorption is possible important for very massive objects in the bright end of LFs, but their contribution to the emissivity is very small. The lack of significant dust absorption is further supported by the observed very blue UV-continuum slopes of high- z galaxies reported in Bouwens et al. (2009). Therefore, we ignore the effect of dust in current calculations. Furthermore, we will show latter that the high- z galaxies are inadequate to explain the amplitude of the observed fluctuations, considering the dust absorption would only strength this point.

that cannot escape into the intergalactic medium (IGM), i.e., $1 - f_{\text{esc}}$, where f_{esc} is the escape fraction. Ionizing photons escaping from galaxies would ionize the IGM; such ionized gas could also produce the nebular emission. However, due to the very low recombination rate, as shown in, e.g., Nakamoto et al. (2001) and Cooray et al. (2012a), its emissivity is much weaker than the radiation from galaxies, so we ignore this contribution in this paper. The IGM contribution to the NIRB fluctuations is also negligible (Fernandez et al. 2010).

To determine the escape fraction averaged over the galaxy populations present at a given redshift, we proceed as follows. First we compute the number of ionizing photons emitted per baryon in collapsed objects as:

$$f_{\star} N_{\gamma} = \frac{\sum_{i=1}^N \left[q_{\text{H}}^{\text{II}}(\tau^{\text{II},i}, Z^i) \dot{M}_{\star}^{\text{II},i} \tau^{\text{II},i} + q_{\text{H}}^{\text{III}} M_{\star}^{\text{III},i} \tau^{\text{III}} \right]}{\sum_{i=1}^N M_{\text{gas}}^i}, \quad (4)$$

where q_{H}^{II} is the emission rate of ionizing photons from Pop II stars (this quantity depends on both the age and the metallicity of the stellar population) corresponding to a continuous star formation rate $1 M_{\odot} \text{yr}^{-1}$. We derive this quantity from the **Starburst99** templates³ (Leitherer et al. 1999; Vázquez & Leitherer 2005; Leitherer et al. 2010) adopting the mean age, $\tau^{\text{II},i}$, and metallicity, Z^i , of each simulated galaxy. $q_{\text{H}}^{\text{III}}$ is the emission rate of ionizing photons for Pop III stars according to Schaerer (2002)⁴. M_{gas}^i is the gas content, $\dot{M}_{\star}^{\text{II},i}$ is the mean star formation rate of Pop II stars in this galaxy, while $M_{\star}^{\text{III},i}$ is the cumulative mass of Pop III stars. We use a mean lifetime $\tau^{\text{III}} = 2.5 \times 10^6$ yr for massive Pop III stars (Schaerer 2002; Salvaterra et al. 2011).

We then compare the above quantity with the number of ionizing photons per baryon in collapsed objects, N_{ion} , required by interpreting the observations as in Mitra et al. (2012) (the “mean” value) to get the escape fraction, i.e., $f_{\text{esc}} = \min(\frac{C N_{\text{ion}}}{f_{\star} N_{\gamma}}, 1.0)$, where C is the clumping factor. Throughout this paper we assume $C = 1$ to get the minimum f_{esc} therefore the maximum contribution of the nebular emission to the NIRB. We note that the clumping factor could be higher than 1 even at high redshifts (Pawlik et al. 2009; Shull et al. 2012). For example, Shull et al. (2012) gives $C \approx 3$ (1.7) at $z = 5$ (9) by numerical simulations. Our nebular emission is therefore reduced by about 10% to 60% from $z = 5$ to $z = 9$ if this clumping factor is adopted. However, for Pop II stars which are the dominant contributors to the NIRB, the nebular emission is much smaller than the stellar emission. So the final reduction in the NIRB would be much smaller. Furthermore, we will show later that the flux from high redshift galaxies and Pop III stars is unable to explain the observed fluctuations level, so that a reduction in the NIRB flux would in any case strengthen this conclusion. We plot the derived f_{esc} as a function of redshift in Figure 1. There is a clear trend of an increasing escape fraction towards higher redshifts; it reaches 1 at $z \approx 11$. At $z = 5$, the final redshift of the simulation, $f_{\text{esc}} \approx 0.05$. Although required by reionization data, an increasing trend

³<http://www.stsci.edu/science/starburst99/docs/default.htm>

⁴Note the different dimensions of q_{H}^{II} and $q_{\text{H}}^{\text{III}}$: the former corresponds to per unit star formation rate while the latter corresponds to per unit stellar mass.

of $f_{\text{esc}}(z)$ has not yet been fully understood theoretically in spite of the several, often conflicting, studies on this problem.

Based on observations, Inoue et al. (2006) concluded that $f_{\text{esc}} > 0.1$ when $z > 4$; by combining the observations of Lyman α absorption and UV LF, and also using N-body simulations and semi-analytical prescriptions to model the ionizing background, Srbinovsky & Wyithe (2010) found that for galaxies at $z \sim 5.5 - 6$, if the minimum mass of star forming galaxies corresponds to the hydrogen cooling threshold, $f_{\text{esc}} \sim 0.05 - 0.1$; Wyithe et al. (2010) used the star formation rate derived from gamma-ray burst observations to conclude that in the redshift range $4 - 8.5$, $f_{\text{esc}} \sim 0.05$; Wise & Cen (2009), by radiation hydrodynamical simulations, found that at redshift 8 for galaxies with $M_{\text{vir}} < 10^{7.5} M_{\odot}$, $f_{\text{esc}} \sim 0.05 - 0.1$, while for more massive galaxies $f_{\text{esc}} \sim 0.4$, if a normal IMF is adopted; also via simulations, Razoumov & Sommer-Larsen (2010) found $f_{\text{esc}} \sim 0.8$ when $z = 10$. The escape fraction derived by us is broadly consistent with these values. The important difference however is that our derivation of f_{esc} matches both the LF and the reionization history simultaneously, i.e., a more phenomenological derivation, so that we can get around the detailed physical mechanisms of the escape fraction. Different from our approach, Mitra et al. (2013) computed the LFs of high redshift galaxies by means of semi-analytical models and derived the star formation efficiency f_{\star} required to match the observed ones. They found $f_{\text{esc}} \approx 0.07$ at $z = 6$ and $f_{\text{esc}} \approx 0.16$ at $z = 7$, which are consistent with our $f_{\text{esc}} \approx 0.06$ (0.18) at those two redshifts. At higher redshifts, however, their escape fraction is somewhat lower than ours.

As a final remark, we underline that when computing the escape fraction, we do not make a distinction between Pop III and Pop II stars. In the calculation of $f_{\star} N_{\gamma}$ ionizing photons from both populations are accounted for, f_{esc} can be regarded as a kind of “effective” escape fraction averaged over the galaxy population. In principle, f_{esc} for Pop III stars should be higher due to their harder spectrum. However, as we will see in Section 3, Pop III stars only contribute a negligible flux to the present-day NIRB, a more detailed modeling is then not necessary.

The luminosity of the i -th galaxy, L_{ν}^i , is the sum of the contribution of Pop II and Pop III stars. For Pop II stars we use the age and metallicity dependent spectrum templates provided by the **Starburst99** code. The nebular emission contribution has been renormalized by adopting the escape fraction computed above. In addition to the free-free, free-bound and two-photon emissions which have already been included in **Starburst99**, we add the Lyman α emission to the template by using (Fernandez & Komatsu 2006)

$$l_{\alpha}(\nu, \tau^{\text{II},i}, Z^i, z) = f_{\alpha} h_{\text{p}} \nu_{\alpha} \phi(\nu - \nu_{\alpha}) q_{\text{H}}^{\text{II}}(\tau^{\text{II},i}, Z^i) [1 - f_{\text{esc}}(z)], \quad (5)$$

in which $f_{\alpha} = 0.64$ (Fernandez & Komatsu 2006), h_{p} is the Plank constant, $\nu_{\alpha} = 2.47 \times 10^{15}$ Hz is the frequency of Lyman α photons. We use the line profile $\phi(\nu - \nu_{\alpha})$ provided in Santos et al. (2002):

$$\phi(\nu - \nu_{\alpha}) = \begin{cases} \nu_{\star}(z)(\nu - \nu_{\alpha})^2 \exp[-\nu_{\star}(z)/|\nu - \nu_{\alpha}|] & \text{if } \nu \leq \nu_{\alpha} \\ 0 & \text{if } \nu > \nu_{\alpha}, \end{cases} \quad (6)$$

where

$$\nu_\star(z) = 1.5 \times 10^{11} \left(\frac{\Omega_b h^2}{0.019} \right) \left(\frac{h}{0.7} \right)^{-1} \frac{(1+z)^3}{\sqrt{\Omega_m(1+z)^3 + \Omega_\Lambda}} \text{ Hz} \quad (7)$$

is the fitted form of results given in Loeb & Rybicki (1999).

For the template of Pop III stars, l_ν^{III} , we still use the spectrum in Schaerer (2002), but renormalize the nebular emission part by the factor $1 - f_{\text{esc}}$. The luminosity of the i -th galaxy is then given by (Salvaterra et al. 2011)

$$L_\nu^i(z) = l_\nu^{\text{II}}(\tau^{\text{II},i}, Z^i, z) \dot{M}_\star^{\text{II},i} + l_\nu^{\text{III}}(z) \dot{M}_\star^{\text{III},i} \tau^{\text{III}}, \quad (8)$$

here the Lyman α emission in Eq. (5) has already been included in l_ν^{II} .

With the luminosity for each galaxy given as above, we can then obtain the emissivity according to Eq. (2). As an example, we plot the $\nu\epsilon(\nu, z)$ at redshifts 12.0, 9.0 and 6.0 respectively in Figure 2. At high redshifts, the escape fraction ≈ 1.0 , yielding a very weak Ly α line, since such emission is produced by recombinations of the ionized nebula around stars. At lower redshifts, the escape fraction drops, while more ionizing photons are absorbed by the material around the stars, and producing more Ly α emission which is more clearly seen in the spectrum.

The part of spectrum with energy below 10.2 eV is of the most interest to us, here the spectrum becomes increasingly flatter at later time. For example, at $z = 12$, the slope of $\nu\epsilon(\nu, z) \propto \nu^\beta$ with $\beta \approx 2$, while at $z = 5$ $\beta \approx 1.2$. This is clearly the result of an aging effect enhancing the rest frame optical/IR bands flux with respect to the UV ones. Since the NIRB from $z > 5$ galaxies is dominated by the lower redshift galaxies ($5 < z < 8$), we do not expect to have a very steep NIRB spectrum, as we will see in the results presented in Sec. 3.

2.2. NIRB Fluctuations

Using the Limber approximation, the angular power spectrum of the fluctuations of the flux field is (Cooray et al. 2012a)

$$C_l = \int_{z_{\text{min}}}^{z_{\text{max}}} \frac{dz}{r^2(z)(1+z)^4} \frac{dr}{dz} [\nu\epsilon(\nu, z) e^{-\tau_{\text{eff}}(\nu_0, z)}]^2 P_{\text{gg}}(k, z), \quad (9)$$

where $r(z)$ is the comoving distance and $P_{\text{gg}}(k, z)$ is the galaxy-galaxy power spectrum, $k = l/r(z)$. In Eq. (9) we assume that the luminous properties of galaxies are independent of their locations, so that the only factor which determines their contribution to the NIRB fluctuations is their spatial fluctuations (see Shang et al. 2012 for an improved model).

The 10 h^{-1} Mpc box size of Salvaterra et al. (2011) simulations is too small to provide us with the large scale correlation function of galaxies (for sources at $z = 6$, the comoving transverse separation corresponding to 1° angular size is about 100 h^{-1} Mpc), so we use the halo model

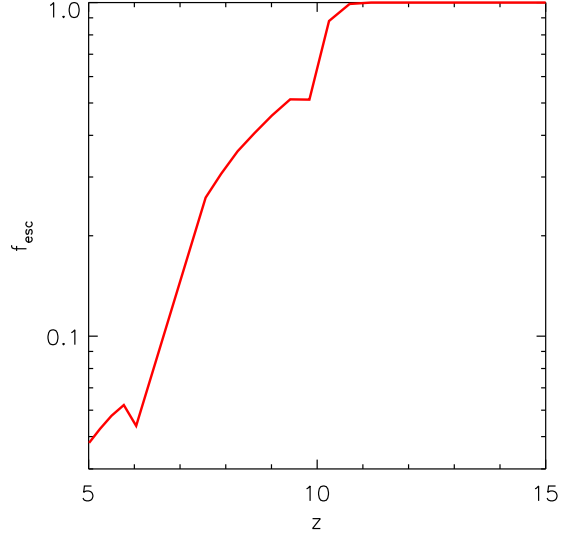


Fig. 1.— Escape fraction evolution from joint LF-reionization constraints.

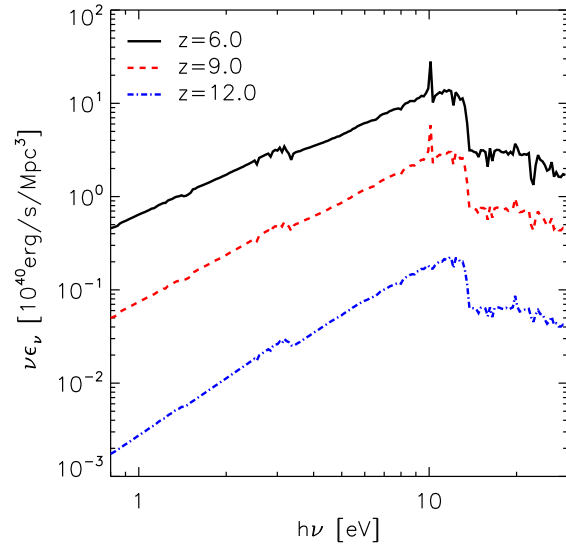


Fig. 2.— The emissivity of simulated galaxies at redshift 12.0 (dash-dotted), 9.0 (dashed) and 6.0 (solid) respectively.

(Cooray & Sheth 2002; Cooray 2004) to calculate the galaxy-galaxy power spectrum. This power spectrum is composed of two parts, the one-halo term from the correlation of galaxies in the same halo (including the central galaxies and satellite galaxies), and the two-halo term from galaxies in different halos:

$$P_{\text{gg}}(k, z) = P_{\text{gg}}^{1h}(k, z) + P_{\text{gg}}^{2h}(k, z). \quad (10)$$

Assuming that the distribution of galaxies in a halo traces the profile of dark matter, and the mean number of central galaxies and satellite galaxies in a halo with mass M are $\langle N_{\text{sat}} \rangle$ and $\langle N_{\text{cen}} \rangle$, respectively, we have

$$P_{\text{gg}}^{1h}(k, z) = \int_{M_{\text{min}}(z)}^{M_{\text{max}}(z)} dM \frac{dn}{dM} \frac{2\langle N_{\text{sat}} \rangle \langle N_{\text{cen}} \rangle u(M, k) + \langle N_{\text{cen}} \rangle^2 u^2(M, k)}{\bar{n}_{\text{gal}}^2}, \quad (11)$$

and

$$P_{\text{gg}}^{2h}(k, z) = P_{\text{lin}}(k, z) \times \left[\int_{M_{\text{min}}(z)}^{M_{\text{max}}(z)} dM \frac{dn}{dM} b(M, z) \frac{\langle N_{\text{sat}} \rangle + \langle N_{\text{cen}} \rangle}{\bar{n}_{\text{gal}}} u(M, k) \right]^2. \quad (12)$$

In the above expressions, $M_{\text{min}}(z)$ is the minimum mass of halos that could host galaxies, and we set it to be the minimum mass of halos that contain stars in our simulations, which is $\sim (2-8) \times 10^7 M_{\odot}$, depending on the redshift. $M_{\text{max}}(z)$ is the maximum mass contributing to the emissivity and the clustering, we will describe how to determine it later, dn/dM is the mass function (Sheth & Tormen 1999; Sheth et al. 2001), while $u(M, k)$ is the normalized Fourier transform of the halo profile. For a NFW profile (Navarro et al. 1997), the analytical expression is given by Cooray & Sheth (2002), and we use the concentration parameter, c_{M} , from Prada et al. (2012) which fits simulations well. However, we find that our results are insensitive to the use of different concentrations, as e.g., from Zehavi et al. (2011). Even if a very different concentration parameter is adopted, its impacts are non-negligible only in the one-halo term which dominates the signal at small scales, where galaxy clustering is well below the shot noise. As we are interested primarily in the large-scale ($> 1'$) clustering, our conclusions are unaffected by the adopted value of c_{M} . Finally, for the halo bias $b(M, z)$ we use the formula and fitted parameters given by Tinker et al. (2010), which is higher than Sheth et al. (2001) for massive halos, but is better fit to simulations. The linear matter power spectrum $P_{\text{lin}}(k, z)$ is taken from Eisenstein & Hu (1998).

The mean number of central galaxies and satellites in a halo with mass M is modeled by the halo occupation distribution (HOD) model (Zheng et al. 2005),

$$\langle N_{\text{cen}} \rangle = \frac{1}{2} \left[1 + \text{erf} \left(\frac{\log_{10} M - \log_{10} M_{\text{min}}}{\sigma_{\log_{10} M}} \right) \right], \quad (13)$$

and

$$\langle N_{\text{sat}} \rangle = \frac{1}{2} \left[1 + \text{erf} \left(\frac{\log_{10} M - \log_{10} 2M_{\text{min}}}{\sigma_{\log_{10} M}} \right) \right] \left(\frac{M}{M_{\text{sat}}} \right)^{\alpha_s}. \quad (14)$$

We adopt the parameters $M_{\text{sat}} = 15M_{\text{min}}$, $\sigma_{\log_{10} M} = 0.2$ and $\alpha_s = 1.0$, which are from both simulations and semi-analytical models (Zheng et al. 2005), and observations (Zehavi et al. 2011).

With the mean number of central and satellite galaxies in each halo, the galaxy number density is simply

$$\bar{n}_{\text{gal}} = \int_{M_{\text{min}}(z)}^{M_{\text{max}}(z)} dM \frac{dn}{dM} (\langle N_{\text{cen}} \rangle + \langle N_{\text{sat}} \rangle). \quad (15)$$

In addition to the above galaxy clustering, Poisson fluctuations in the number of galaxies would generate shot noise in observations, whose power spectrum dominates at small scales. If the redshift derivative of the number of sources with flux between S and $S + dS$ is $\frac{d^2 N}{dS dz}$, the angular power spectrum of such shot noise is

$$C_l^{\text{SN}} = \frac{1}{\Delta\Omega} \int dz \int dS S^2 \frac{d^2 N}{dS dz} = \frac{1}{\Delta\Omega} \int dz \int dM S^2 \frac{d^2 N}{dM dz}, \quad (16)$$

where $\Delta\Omega$ is the beam angle. Considering that

$$\frac{d^2 N}{dM dz} = \frac{dn}{dM} \Delta\Omega r^2 \frac{dr}{dz}, \quad (17)$$

and

$$S = \frac{L_\nu(M) e^{-\tau_{\text{eff}}(\nu_0, z)}}{4\pi r^2 (1+z)}, \quad (18)$$

where $L_\nu(M)$ is the luminosity of halos with mass M , the shot noise power spectrum is

$$C_l^{\text{SN}} = \int dz \frac{e^{-\tau_{\text{eff}}(\nu_0, z)}}{r^2 (1+z)^2} \frac{dr}{dz} \int \left[\frac{L_\nu(M)}{4\pi M} \right]^2 M^2 \frac{dn}{dM} dM. \quad (19)$$

As we assume the luminous properties of galaxies are independent of their location, in the square bracket we can simply use an average light-to-mass ratio that is independent of the halo mass,

$$\frac{1}{4\pi} \int L_\nu(M) \frac{dn}{dM} dM \bigg/ \int M \frac{dn}{dM} dM = \frac{\epsilon(\nu, z)}{\rho_h}. \quad (20)$$

We finally obtain the shot noise angular power spectrum

$$C_l^{\text{SN}} = \int_{z_{\text{min}}}^{z_{\text{max}}} \frac{cdz}{H(z)r^2(z)(1+z)^4} P^{\text{SN}}(z), \quad (21)$$

where

$$P^{\text{SN}}(z) = \left[\frac{\nu \epsilon(\nu, z) e^{-\tau_{\text{eff}}}}{\rho_h} \right]^2 \int_{M_{\text{min}}(z)}^{M_{\text{max}}(z)} dM M^2 \frac{dn}{dM}, \quad (22)$$

and the halo mass density is

$$\rho_h = \int_{M_{\text{min}}(z)}^{M_{\text{max}}(z)} dM M \frac{dn}{dM}$$

.

In observations, the detected sources are generally removed down to a certain limiting magnitude, m_{lim} , the residue is the source-subtracted NIRB fluctuations. To simulate this, we also

remove bright galaxies in the simulation box and in the bright-end. In theoretical calculations, this limiting magnitude is determined by letting the predicted shot noise level match the values found in the measurements.

The apparent limiting magnitude (at wavelength λ_0) is converted into the rest frame absolute magnitude (at wavelength $\lambda_0/(1+z)$) $M_{\lambda_0/(1+z)}$ by

$$M_{\lambda_0/(1+z)} = m_{\text{lim}} - DM(z) + 2.5\log_{10}(1+z), \quad (23)$$

where $DM(z)$ is the distance modulus (Helgason et al. 2012). By using a light-to-mass ratio constructed from the simulation, we determine the maximum halo mass $M_{\text{max}}(z)$. Things are slightly more complicated when calculating the absolute flux and the spectrum of fluctuations, since they both depend on wavelength, while the limiting magnitude in observations at different wavelength is different. In this case we simply give the theoretical prediction without removing any sources in the simulation box and the bright-end, as shown in Figure 3 and Figure 7, corresponding to $M_{\text{max}} = \infty$. Then we discuss the effects of galaxy removal, i.e., in Figure 4. Throughout this paper we adopt $z_{\text{min}} = 5$ and $z_{\text{max}} = 19$ unless otherwise specified.

3. RESULTS

We start by presenting the contribution of high- z galaxies to the absolute flux of the NIRB observed at $z = 0$ in the (observer frame) wavelength range $0.3 - 10 \mu\text{m}$. Figure 3 (top panel) shows the predicted cumulative flux when all sources with $z > 5$ are included; also shown separately are the contributions from Pop II and Pop III stars. The flux peak value is $0.2 \text{ nW/m}^2/\text{sr}$ at $\lambda_0 = 0.9 \mu\text{m}$, and decreases to $0.04 \text{ nW/m}^2/\text{sr}$ at $\lambda_0 = 4.5 \mu\text{m}$. The small bump on the left side of the peak is due to intergalactic Ly α absorption by intervening neutral hydrogen.

We find that in our case, the Pop III contribution is almost negligible (it never exceeds 1%). This is not surprising, for in the simulation the Pop III star formation rate is about three orders of magnitude lower than that of Pop II stars at $z = 10$; the ratio is even smaller below this redshift (Tornatore et al. 2007b). Stated differently, halos with the highest Pop III stellar fraction are usually smaller and less luminous, and their contribution to the total luminosity is very low (Salvaterra et al. 2011). This means that it is very difficult to find Pop III signatures by means of NIRB observations.

In the bottom panel of Figure 3, we plot the contributions from the sources above redshift 5.0, 8.0 and 12.0, respectively. From the figure, it is clear that the contributions from the sources at $5 < z < 8$ dominate, providing about 90% of the flux from all sources with $z > 5$. Most of these sources are the low-luminosity galaxies which cannot be detected individually in current surveys, and they are believed to be the major contributors to reionization. In principle, then, the NIRB could be a perfect tool to study the reionization sources without detecting them individually.

One way to approach the high- z components is to remove bright sources in the field of view.

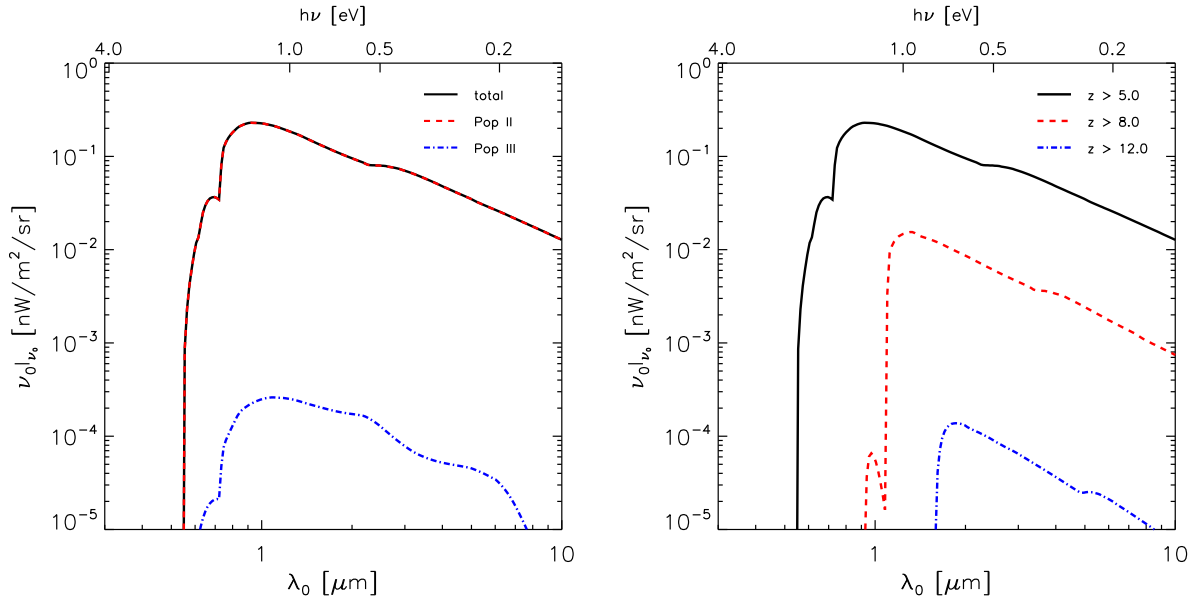


Fig. 3.— The NIRB flux from high- z galaxies, $\nu_0 I_{\nu_0}$, as a function of wavelength in the observer frame. *Left panel:* Contributions from Pop II (dashed line), Pop III (dash-dotted) stars, and their sum. Since the contribution from Pop III stars is very small, the solid line and the dashed line are almost identical. *Right panel:* Contributions from sources in different redshift ranges: $z > 5$ (solid line), $z > 8$ (dashed) and $z > 12$ (dash-dotted).

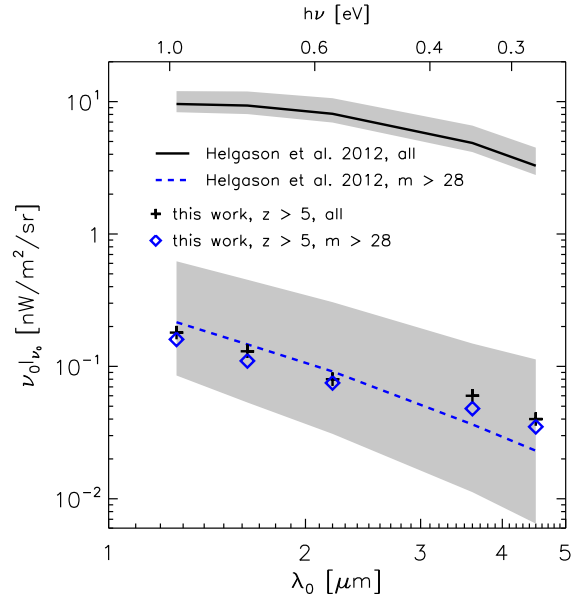


Fig. 4.— NIRB flux in the $1.25 \mu\text{m}$ to $4.5 \mu\text{m}$ wavelength range. The solid line is the flux from all galaxies from the “default” model in Helgason et al. (2012), while the dashed line is the remaining flux after removal of all sources brighter than $m_{\text{lim}} = 28$. The grey regions refer to the flux range between the “HFE” and “LFE” models in Helgason et al. (2012). As a comparison, we plot the flux from all galaxies with $z > 5$ in our work (crosses), and the flux after removal of sources down to $m_{\text{lim}} = 28$ (diamonds). Before any galaxy removal, the flux from galaxies with $z > 5$ is only a few percent of the overall flux in Helgason et al. (2012), i.e. the low- z galaxies dominate. However, after removal of galaxies with $m_{\text{lim}} < 28$, the flux from the remaining galaxies at all redshifts in Helgason et al. (2012) is comparable with that from the remaining galaxies with $z > 5$ in our work.

We plot the flux before and after removal of bright galaxies in Figure 4 at wavelengths from $1.25 \mu\text{m}$ to $4.5 \mu\text{m}$, corresponding to the J through M bands. The crosses refer to flux from all galaxies with $z > 5$ in our work, while the solid line corresponds to the flux from all galaxies at all redshifts in the “default” model of Helgason et al. (2012). After removal of galaxies brighter than $m_{\text{lim}} = 28$, the flux from $z > 5$ galaxies in our work is shown by diamonds, while flux from remaining galaxies in Helgason et al. (2012) is shown by the dashed line. The flux from all galaxies (solid line) is about 1-2 orders of magnitude larger than that from galaxies with $z > 5$ (crosses) in our work. Hence, without bright galaxy removal, $z < 5$ galaxies largely dominate the NIRB flux. However, if we remove the galaxies down to $m_{\text{lim}} = 28$, the flux from the remaining galaxies at all redshifts in Helgason et al. (2012) (dashed line) is comparable to that from the remaining galaxies with $z > 5$ in our work. Even considering the uncertainties on the faint-end of LFs (the shaded regions), in the source-subtracted flux, galaxies at $z > 5$ still contribute at least $\sim 20\% - 30\%$ of the flux from galaxies at all redshifts and fainter than $m = 28$. So at least in principle we can access the signal of reionization sources by subtracting the bright galaxies from the NIRB.

Before moving to fluctuations, we emphasize that the expected contribution of high- z galaxies (including Pop III stars) to the NIRB flux is very small compared with the residual flux in the measurement of Matsumoto et al. (2005). These sources largely fall short of accounting for such residual ($\sim 60 - 6 \text{ nW/m}^2/\text{sr}$ in the wavelength range $1.4 - 4 \mu\text{m}$). It has to be reminded that the flux measured by Matsumoto et al. is likely to be still dominated by incomplete zodiacal light subtraction, as discussed by Thompson et al. (2007a), who concluded that no residual flux is present. Considering the difficulties in modeling the zodiacal light accurately, currently the residual flux measurements are not very useful to constrain models. Therefore, we will base all the conclusions in the present paper on the analysis of fluctuations only, see below.

The fluctuations of the NIRB after subtracting galaxies down to the detection limits of observations, $\sqrt{l(l+1)C_l/(2\pi)}$, at $\lambda_0 = 1.6, 2.4, 3.6, 4.5 \mu\text{m}$ are shown by the thick solid line in each panel of Figure 5. The contribution from $z > 5$ faint galaxies, which is studied in this work, and the contribution from $z < 5$ galaxies, which is calculated by following the reconstruction of Helgason et al. (2012), are shown by dashed line and dash-dotted line respectively. Unless the limiting magnitude is very faint so that the relative fraction of the contribution of high- z galaxies is larger as in the upper left panel, the contribution of $z > 5$ galaxies is negligible compared with the $z < 5$ galaxies, i.e., the total amplitude (solid line) coincides with that of $z < 5$ galaxies (dash-dotted line). To account for the uncertainties of the faint-end of LFs, Helgason et al. (2012) considered two models of the faint end of LFs (adopted for low- z faint galaxies here) which are likely to bracket the real case. Considering this we show the range of the total power spectrum by shaded regions. We also plot observations at corresponding wavelength in each panel by filled circles with errorbars, which are from Thompson et al. (2007a) ($1.6 \mu\text{m}$), Matsumoto et al. (2011) ($2.4 \mu\text{m}$), Cooray et al. (2012b) (3.6 and $4.5 \mu\text{m}$) respectively. The measurements of Cooray et al. (2012b) agree well with observations of Kashlinsky et al. (2012) at the same wavelength, but extend to larger angular scales. In the theoretical predictions, we remove the bright sources by selecting

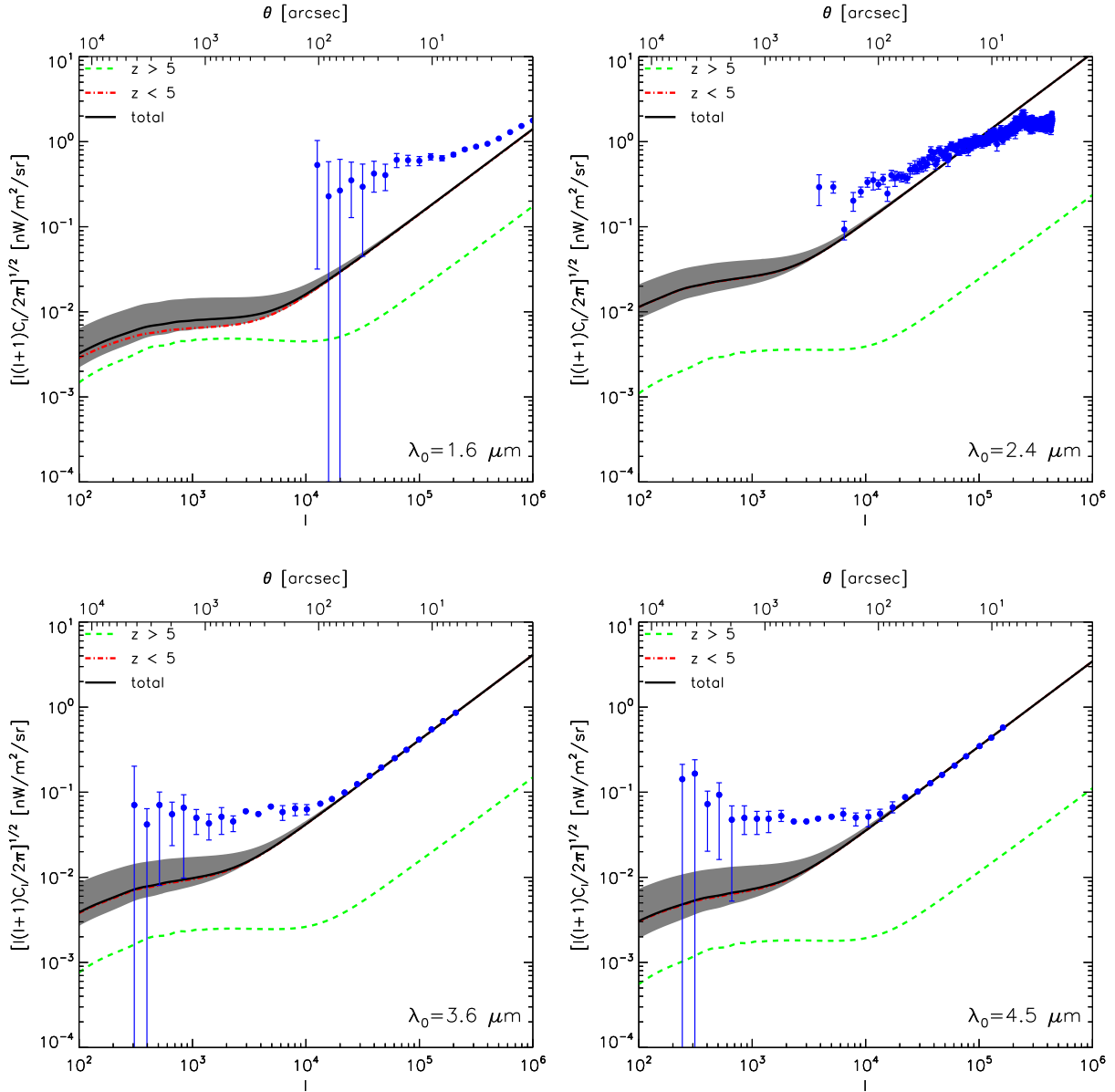


Fig. 5.— NIRB fluctuations angular power spectrum at different (observer frame) wavelengths, as labeled in each panel, both the galaxy clustering and the shot noise are included. The dashed lines represent the contribution from high- z galaxies studied in this work, while the dash-dotted lines represent the contribution from low- z galaxies reconstructed by Helgason et al. (2012) (their “default” model). The solid lines are the sum of these. Note that in all panels except the upper left one where the limiting magnitude is very faint, the dash-dotted line and the solid line are almost identical. The shaded regions are the range of the total power spectrum when considering the different faint end of the LFs which are likely to bracket the real case (the “HFE” and “LFE” models in Helgason et al. 2012). We also plot the observations at wavelength $1.6 \mu\text{m}$ (Thompson et al. 2007a), $2.4 \mu\text{m}$ (Matsumoto et al. 2011), $3.6 \mu\text{m}$ and $4.5 \mu\text{m}$ (Cooray et al. 2012b, which agrees well with another recent measurements, i.e., Kashlinsky et al. 2012, but extends to larger angular scales) by filled circles with errorbars. In all our theoretical predictions we have already removed the bright sources to reach the shot noise level that matches each measurement, see text.

a limiting magnitude at each wavelength to get a shot noise level of the remaining fainter galaxies (including both low- z and high- z ones, but the latter is almost negligible) that matches each measurement, i.e., $m_{\text{lim}} = 26.7, 23.2, 23.9$ and 23.8 respectively, the first two values are the same as Helgason et al. (2012).

At small scales where the shot noise dominates, the model predictions should match the observations, as shown in the 3.6 and $4.5 \mu\text{m}$ panels. In the $2.4 \mu\text{m}$ panel, there is some discrepancy at small scales, this is because the suppression of the power by beam effects is not corrected in the observations data. For the $1.6 \mu\text{m}$ case, a footnote in Helgason et al. (2012) noted that the images at other wavelength are used to subtract bright sources, so there would be spread on the limiting magnitudes.

From the figure, we also see that the contributions of the $z > 5$ galaxies (dashed lines) exceed the shot noise level on large angular scales ($l < 10^4$), this means that the NIRB fluctuations do have the potential to provide us information on the nature of the undetected reionization sources. However, the predicted amplitudes are only $\sim (2-4) \times 10^{-3} \text{ nW/m}^2/\text{sr}$, which is even much smaller than the contribution from low- z faint galaxies, and both the high- z and low- z contributions are much smaller than the observed values, which are at the $\sim 0.1 \text{ nW/m}^2/\text{sr}$ level. Even considering the uncertainties about the faint-end of LFs, the difference is still quite significant, again indicates the existence of one or more unknown component(s) we are missing. Somewhat surprisingly but interestingly, the missing component has a clustering signal very similar to that of the high redshift galaxies, and extends to degree angular scales. Obviously, this component/foreground must be identified before we can make further progress and use the NIRB to study reionization sources.

Next, we define the fluctuation amplitude $\delta F = \sqrt{l(l+1)C_l/(2\pi)}$, and plot its ratio to $F = \nu_0 I_{\nu_0}$ in Figure 6. Such relative fluctuation is almost independent of λ_0 (see also Fernandez et al. 2010), $\delta F/F \sim 4\%$ at $l = 2000$, with the only slight deviation of the $1.6 \mu\text{m}$ band where it is somewhat lower than in redder bands, as a consequence of a deeper ($m_{\text{lim}} \approx 27$) galaxy removal. Nicely, the relative fluctuation agrees with that found by Fernandez et al. (2010) and Cooray et al. (2012a). In addition, $\delta F/F$ increases with z_{min} , i.e., high redshift sources have higher relative fluctuations. For example, $\delta F/F = 7\%$ for $z_{\text{min}} = 8.0$, while it reaches 12% if $z_{\text{min}} = 12.0$ is adopted. It reflects the more biased spatial distributions of higher redshift sources. The relative fluctuation $\delta F/F$ is only weakly dependent on the intrinsic properties of galaxies (Fernandez et al. 2010), but more so on the spatial clustering features. Thus, $\delta F/F$ is a key indicator to identify NIRB sources; yet, in practice, it is hard to get an accurate absolute flux.

The spectrum of the fluctuations, $\delta F(\lambda_0)$ from all galaxies with $z > 5$ at $l = 2000$, shown in Figure 7, has a slope λ_0^p , with $p = -1.4$ above $1 \mu\text{m}$. Such slope is essentially the same as that of the flux, reflecting the above mentioned wavelength independency of $\delta F/F$.

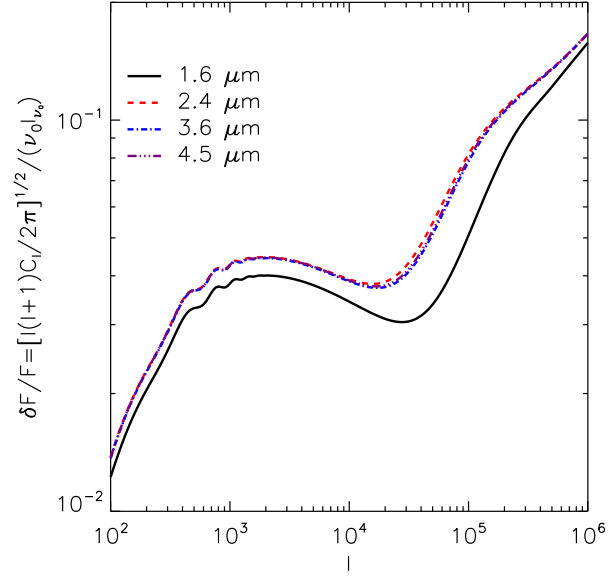


Fig. 6.— The ratio of $\delta F/F$ as a function of l for four different wavelengths.

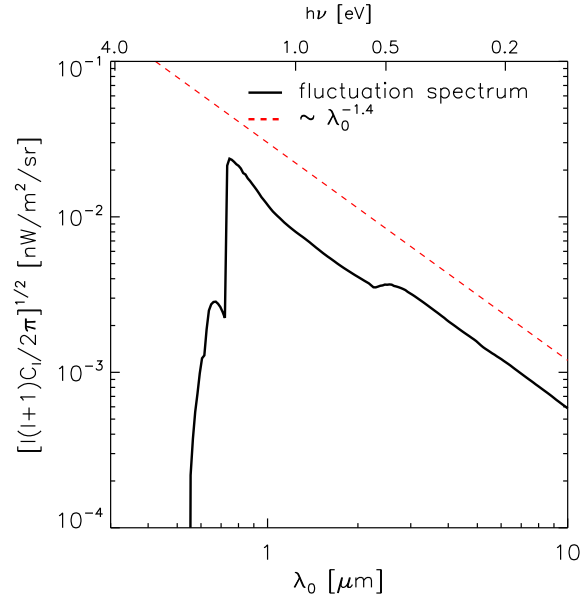


Fig. 7.— The spectrum of the NIRB (contributed by all $z > 5$ galaxies) fluctuations (solid line) at $l = 2000$, the dashed line shows a $\lambda_0^{-1.4}$ law.

4. CONCLUSIONS

By combining high resolution cosmological N-body/hydrodynamical simulations and an analytical model, we predicted the contributions to the absolute flux and fluctuations of the NIRB by high redshift ($z > 5$) galaxies, some of which harboring Pop III stars. This is the most robust and detailed theoretical calculation done so far, as we simultaneously match the LFs and reionization constraints. The simulations include the relevant physics of galaxy formation and a novel treatment of chemical feedback, by following the metallicity evolution and implementing the physics of Pop III/Pop II transition based on a critical metallicity criterion. It reproduces the observed UV LFs over the redshift range $5 < z < 10$, and extend it to faint magnitudes far below the detection limit of current observations.

We directly calculate the stellar emissivity from the simulations. We use `Starburst99` to generate metallicity and age dependent SED templates, then calculate the luminosity for each galaxy according to its current star formation rate, stellar age and metallicity, instead of using a constant metallicity and average main sequence spectrum template. Except for the mass range of the IMF which has already been fixed in the simulation, there are no other free parameters in the calculation of the emissivity.

By comparing the number of ionizing photons produced per baryon in collapsed objects, $f_{\star}N_{\gamma}$, in the simulation and the ionizing photon rate $N_{\text{ion}} \approx f_{\text{esc}}f_{\star}N_{\gamma}$ deduced from observationally constrained reionization models, we obtained the evolution history of the escape fraction of ionizing photons, $f_{\text{esc}}(z)$. We find $f_{\text{esc}} \approx 1$ at $z > 11$, decreasing to ≈ 0.05 at $z = 5$. This escape fraction is used to renormalize the nebular emission of Pop III and Pop II stars in the emissivity.

Pop III stars are unlikely to be responsible for the observed NIRB residual, and their contribution is very small, making up $< 1\%$ of the total absolute flux in our calculation. This is the natural result of the much lower star formation rate of Pop III stars compared with Pop II stars in the simulation, since even metals from a single Pop III star could enrich above the critical metallicity a large amount of gas around it (Tornatore et al. 2007b). The formation of Pop III stars is regulated by such a chemical feedback mechanism, which limits their contribution to the NIRB. However, a rapid Pop III-Pop II transition brings also a little advantage in terms of integrated emissivity, due to the longer lifetime of Pop II stars (Cooray et al. 2012a).

We predict that in the wavelength range $1.0 - 4.5 \mu\text{m}$, the NIRB flux from $z > 5$ galaxies (and their Pop III stars) is $\sim 0.2 - 0.04 \text{ nW/m}^2/\text{sr}$, while the fluctuation strength is about $\delta F = 0.01 - 0.002 \text{ nW/m}^2/\text{sr}$ at $l = 2000$. If we remove galaxies down to $m_{\text{lim}} = 28$, the above flux level is only slightly reduced; however, by comparing with Helgason et al. (2012), we find that the flux from $z < 5$ dramatically decreases and the remaining becomes comparable to the predicted signal of $z > 5$ galaxies. This implies that in principle it is possible to get the signal from reionization sources by subtracting galaxies down to a certain magnitude.

The relative fluctuation amplitude, $\delta F/F$, at $l = 2000$ is $\sim 4\%$, almost independent of the

wavelength. This ratio may be helpful to investigate the clustering features of the sources contribute to the NIRB, since the intrinsic properties of galaxies almost cancel out. Despite the difficulties in measuring the absolute flux accurately, it could be treated as a quality indicator in the data reduction process: if a much higher/lower ratio is obtained from the data, this might suggest that a more careful analysis work is required to extract the genuine contribution from reionization sources.

In spite of being accurate and consistent with the observed LFs and reionization data, thus offering a robust prediction of the NIRB contribution from high- z galaxies which likely reionized the universe, a puzzling question remains: the predicted fluctuations are considerably lower than the observed values, indicating that in addition to the contribution from the expected high- z galaxy population (and Pop III stars), we should invoke some other – yet unknown – missing component(s) or foreground(s) which dominates the currently observed source-subtracted NIRB. Moreover, the angular clustering of this missing component must be very similar to that of the high redshift galaxies and extends to degree scales. Obviously, this component/foreground must be identified and removed before we are ready to exploit the NIRB to study reionization sources. On the other hand, sources located at $5 < z < 8$ provide about 90% of the flux from all sources with $z > 5$ in our simulation; most of them are the faint galaxies currently undetected by deep surveys. Thus, if the above mentioned additional spurious sources/foregrounds can be removed reliably, the NIRB will become the primary tool to investigate the properties of the reionizing sources.

ACKNOWLEDGMENTS

It is a pleasure to acknowledge intense discussions and data exchange with A. Cooray, K. Helgason, E. Komatsu, T. Matsumoto, R. Thompson, S. Kashlinsky, S. Mitra and T. Choudhury. AF thanks UT Austin for support and hospitality as a Centennial B. Tinsley Professor and the stimulating atmosphere of the NIRB Workshop organized by the Texas Cosmology Center. BY and XC also acknowledges the support of the NSFC grant 11073024, the MoST Project 863 grant 2012AA121701, and the Chinese Academy of Science Knowledge Innovation grant KJCX2-EW-W01.

REFERENCES

- Bouwens, R. J. et al. 2009, *ApJ*, 705, 936
- Bouwens, R. J., Illingworth, G. D., Franx, M., & Ford, H. 2007, *ApJ*, 670, 928
- Bouwens, R. J. et al. 2011a, *Nature*, 469, 504
- . 2011b, *ApJ*, 737, 90
- . 2010, *ApJ*, 709, L133

- Cambrésy, L., Reach, W. T., Beichman, C. A., & Jarrett, T. H. 2001, *ApJ*, 555, 563
- Chary, R.-R., Cooray, A., & Sullivan, I. 2008, *ApJ*, 681, 53
- Choudhury, T. R., & Ferrara, A. 2007, *MNRAS*, 380, L6
- Cooray, A. 2004, *MNRAS*, 348, 250
- Cooray, A., Bock, J. J., Keatin, B., Lange, A. E., & Matsumoto, T. 2004, *ApJ*, 606, 611
- Cooray, A., Gong, Y., Smidt, J., & Santos, M. G. 2012a, *ApJ*, 756, 92
- Cooray, A., & Sheth, R. 2002, *Phys. Rep.*, 372, 1
- Cooray, A. et al. 2012b, *Nature*, 490, 514
- . 2007, *ApJ*, 659, L91
- Dwek, E., & Arendt, R. G. 1998, *ApJ*, 508, L9
- Dwek, E., Arendt, R. G., & Krennrich, F. 2005, *ApJ*, 635, 784
- Eisenstein, D. J., & Hu, W. 1998, *ApJ*, 496, 605
- Fernandez, E. R., Iliev, I. T., Komatsu, E., & Shapiro, P. R. 2012, *ApJ*, 750, 20
- Fernandez, E. R., & Komatsu, E. 2006, *ApJ*, 646, 703
- Fernandez, E. R., Komatsu, E., Iliev, I. T., & Shapiro, P. R. 2010, *ApJ*, 710, 1089
- Finkelstein, S. L. et al. 2012, *ApJ*, 758, 93
- Girardi, L., Bressan, A., Bertelli, G., & Chiosi, C. 2000, *A&AS*, 141, 371
- Gorjian, V., Wright, E. L., & Chary, R. R. 2000, *ApJ*, 536, 550
- Helgason, K., Ricotti, M., & Kashlinsky, A. 2012, *ApJ*, 752, 113
- Hosokawa, T., Omukai, K., Yoshida, N., & Yorke, H. W. 2011, *Science*, 334, 1250
- Inoue, A. K., Iwata, I., & Deharveng, J.-M. 2006, *MNRAS*, 371, L1
- Jaacks, J., Choi, J.-H., Nagamine, K., Thompson, R., & Varghese, S. 2012, *MNRAS*, 420, 1606
- Kashlinsky, A. 2005, *Phys. Rep.*, 409, 361
- Kashlinsky, A., Arendt, R., Gardner, J. P., Mather, J. C., & Moseley, S. H. 2004, *ApJ*, 608, 1
- Kashlinsky, A., Arendt, R. G., Ashby, M. L. N., Fazio, G. G., Mather, J., & Moseley, S. H. 2012, *ApJ*, 753, 63

- Kashlinsky, A., Arendt, R. G., Mather, J., & Moseley, S. H. 2005, *Nature*, 438, 45
- . 2007a, *ApJ*, 654, L5
- . 2007b, *ApJ*, 654, L1
- Kashlinsky, A., Odenwald, S., Mather, J., Skrutskie, M. F., & Cutri, R. M. 2002, *ApJ*, 579, L53
- Komatsu, E. et al. 2011, *ApJS*, 192, 18
- Leitherer, C., Ortiz Otálvaro, P. A., Bresolin, F., Kudritzki, R.-P., Lo Faro, B., Pauldrach, A. W. A., Pettini, M., & Rix, S. A. 2010, *ApJS*, 189, 309
- Leitherer, C. et al. 1999, *ApJS*, 123, 3
- Loeb, A., & Rybicki, G. B. 1999, *ApJ*, 524, 527
- Lorenzoni, S., Bunker, A. J., Wilkins, S. M., Stanway, E. R., Jarvis, M. J., & Caruana, J. 2011, *MNRAS*, 414, 1455
- Madau, P., & Silk, J. 2005, *MNRAS*, 359, L37
- Magliocchetti, M., Salvaterra, R., & Ferrara, A. 2003, *MNRAS*, 342, L25
- Matsumoto, T. et al. 2000, in *Lecture Notes in Physics*, Berlin Springer Verlag, Vol. 548, ISO Survey of a Dusty Universe, ed. D. Lemke, M. Stickel, & K. Wilke, 96
- Matsumoto, T. et al. 2005, *ApJ*, 626, 31
- . 2011, *ApJ*, 742, 124
- Mitra, S., Choudhury, T. R., & Ferrara, A. 2012, *MNRAS*, 419, 1480
- Mitra, S., Ferrara, A., & Choudhury, T. R. 2013, *MNRAS*, 428, L1
- Nakamoto, T., Umemura, M., & Susa, H. 2001, *MNRAS*, 321, 593
- Navarro, J. F., Frenk, C. S., & White, S. D. M. 1997, *ApJ*, 490, 493
- Oesch, P. A. et al. 2010, *ApJ*, 709, L16
- Pawlik, A. H., Schaye, J., & van Scherpenzeel, E. 2009, *MNRAS*, 394, 1812
- Prada, F., Klypin, A. A., Cuesta, A. J., Betancort-Rijo, J. E., & Primack, J. 2012, *MNRAS*, 423, 3018
- Razoumov, A. O., & Sommer-Larsen, J. 2010, *ApJ*, 710, 1239
- Salpeter, E. E. 1955, *ApJ*, 121, 161

- Salvaterra, R., & Ferrara, A. 2003, MNRAS, 339, 973
- . 2006, MNRAS, 367, L11
- Salvaterra, R., Ferrara, A., & Dayal, P. 2011, MNRAS, 414, 847
- Salvaterra, R., Haardt, F., & Ferrara, A. 2005, MNRAS, 362, L50
- Salvaterra, R., Magliocchetti, M., Ferrara, A., & Schneider, R. 2006, MNRAS, 368, L6
- Santos, M. R., Bromm, V., & Kamionkowski, M. 2002, MNRAS, 336, 1082
- Schaerer, D. 2002, A&A, 382, 28
- Schechter, P. 1976, ApJ, 203, 297
- Shang, C., Haiman, Z., Knox, L., & Oh, S. P. 2012, MNRAS, 421, 2832
- Sheth, R. K., Mo, H. J., & Tormen, G. 2001, MNRAS, 323, 1
- Sheth, R. K., & Tormen, G. 1999, MNRAS, 308, 119
- Shull, J. M., Harness, A., Trenti, M., & Smith, B. D. 2012, ApJ, 747, 100
- Srbínovsky, J. A., & Wyithe, J. S. B. 2010, PASA, 27, 110
- Thompson, R. I., Eisenstein, D., Fan, X., Rieke, M., & Kennicutt, R. C. 2007a, ApJ, 657, 669
- . 2007b, ApJ, 666, 658
- Tinker, J. L., Robertson, B. E., Kravtsov, A. V., Klypin, A., Warren, M. S., Yepes, G., & Gottlöber, S. 2010, ApJ, 724, 878
- Tornatore, L., Borgani, S., Dolag, K., & Matteucci, F. 2007a, MNRAS, 382, 1050
- Tornatore, L., Ferrara, A., & Schneider, R. 2007b, MNRAS, 382, 945
- Totani, T., Yoshii, Y., Iwamuro, F., Maihara, T., & Motohara, K. 2001, ApJ, 550, L137
- Vázquez, G. A., & Leitherer, C. 2005, ApJ, 621, 695
- Wise, J. H., & Cen, R. 2009, ApJ, 693, 984
- Wyithe, J. S. B., Hopkins, A. M., Kistler, M. D., Yüksel, H., & Beacom, J. F. 2010, MNRAS, 401, 2561
- Zehavi, I. et al. 2011, ApJ, 736, 59
- Zheng, Z. et al. 2005, ApJ, 633, 791

A. AN ANALYTICAL DERIVATION OF THE EMISSIVITY

At redshift z , the comoving emissivity of stellar population at frequency ν is given by the following integral (Fernandez & Komatsu 2006):

$$\epsilon(\nu, z) = \frac{1}{4\pi} \int_{m_1}^{m_2} L_\nu(m) n_\star(m) dm, \quad (\text{A1})$$

where $L_\nu(m)$ is the specific luminosity of a star with mass m , m_1 is the minimum mass of stars while m_2 is the maximum mass, $n_\star(m)$ is the number density of *shining* stars between m and $m + dm$, which is written as

$$n_\star(m) = \int_{t(z)-\tau(m)}^{t(z)} \dot{n}_\star(m, t') dt', \quad (\text{A2})$$

where $t(z)$ is the age of the universe at redshift z , $\tau(m)$ is the lifetime of a star with mass m . For Pop II stars with metallicity $1/50 Z_\odot$, useful fitting formulae for these quantities as a function of m are collected in Fernandez & Komatsu (2006). Eq. (A2) means that only stars formed between $t(z) - \tau(m)$ and $t(z)$ emit photons at time $t(z)$. The formation rate of stars with mass between m and $m + dm$, $\dot{n}_\star(m, t')$, is

$$\dot{n}_\star(m, t') = \frac{\dot{\rho}_\star(t')}{m_\star} f(m), \quad (\text{A3})$$

in which $f(m)$ is the normalized stellar IMF, i.e., $\int_{m_1}^{m_2} f(m) dm = 1$ and $m_\star = \int_{m_1}^{m_2} m f(m) dm$, while

$$\dot{\rho}_\star(t') = f_\star \frac{\Omega_b}{\Omega_m} \int_{M_{\min}}^{\infty} M \frac{d^2 n}{dM dt'}(M, t') dM \quad (\text{A4})$$

is the comoving star formation rate density in halos with mass above M_{\min} , provided a fraction f_\star of baryons are converted into stars.

Two approximate solutions can be found under particular circumstances. If the star formation rate is almost constant over the time interval $\tau(m)$, i.e., $\tau(m) < t_{\text{SF}}(z)$, where the star formation time scale $t_{\text{SF}}(z) = \left[\frac{\dot{\rho}_\star(z)}{\rho_\star} \right]^{-1}$, then we can make ‘‘Approximation 1’’, i.e.,

$$\int_{t(z)-\tau(m)}^{t(z)} \dot{\rho}_\star(t') dt' \approx \dot{\rho}_\star[t(z)] \tau(m),$$

and the emissivity is approximated as (Fernandez & Komatsu 2006; Fernandez et al. 2010)

$$\epsilon(\nu, z) = \frac{1}{4\pi} \frac{\dot{\rho}_\star(z)}{m_\star} \int_{m_1}^{m_2} L_\nu(m) \tau(m) f(m) dm, \quad (\text{A5})$$

which is usually used for relative massive stars with short lifetime.

On the other hand, if $\tau(m)$ is longer than the age of the universe (this is true for stars of smaller mass, and means that no stars die), then we can use ‘‘Approximation 2’’,

$$\int_{t(z)-\tau(m)}^{t(z)} \frac{\dot{\rho}_\star(t')}{m_\star} dt' = \int_0^{t(z)} \frac{\dot{\rho}_\star(t')}{m_\star} dt' = \frac{\rho_\star(z)}{m_\star}, \quad (\text{A6})$$

the emissivity becomes (Fernandez & Komatsu 2006)

$$\epsilon(\nu, z) = \frac{1}{4\pi} \frac{\rho_\star(z)}{m_\star} \int_{m_1}^{m_2} L_\nu(m) f(m) dm. \quad (\text{A7})$$

This also holds true if $\tau(m)$ is much longer than the star formation time scale $t_{\text{SF}}(z)$, i.e. the death of stars is less significant compared with the formation of new stars, so that

$$\int_{t(z)-\tau(m)}^{t(z)} \frac{\dot{\rho}_\star(t')}{m_\star} dt' = \frac{\Delta\rho_\star(z)}{m_\star} \approx \frac{\rho_\star(z)}{m_\star}, \quad (\text{A8})$$

and the emissivity could also be approximated as Eq. (A7).

In reality, a galaxy is composed of stars with different mass; some of them may have lifetime longer than t_{SF} , while others not. In this case a ‘‘Hybrid’’ approximation could be used,

$$\epsilon(\nu, z) = \frac{1}{4\pi} \left[\frac{\rho_\star(z)}{m_\star} \int_{m_1}^{m_t} L_\nu(m) f(m) dm + \frac{\dot{\rho}_\star(z)}{m_\star} \int_{m_t}^{m_2} L_\nu(m) \tau(m) f(m) dm \right], \quad (\text{A9})$$

where m_t is the stellar mass determined by the condition $\tau(m_t) = t_{\text{SF}}$.

We compare the full analytical solution of Eqs. (A1-A4) with these three approximate solutions. Furthermore, we will also consider the emissivity obtained by adopting the **Starburst99** template at $Z = 1/50 Z_\odot$ instead of the simplified fitting formula given in Fernandez & Komatsu (2006). In this case the emissivity is given by

$$\epsilon(\nu, z) = \frac{1}{4\pi} \int_0^{t(z)} L_{\nu, \text{SB99}}[z, t(z) - t'] \dot{\rho}_\star(t') dt', \quad (\text{A10})$$

where $L_{\nu, \text{SB99}}$ is the luminosity per unit mass (note that here for integration purposes we use the burst star formation model) from **Starburst99**.

In our work, the mass range of Pop II stars is $0.1 - 100 M_\odot$, while the fitted formula of the main sequence age used in Fernandez & Komatsu (2006), Fernandez et al. (2010) and Cooray et al. (2012a) (taken from Schaerer 2002) is based on data of massive stars. To avoid introducing more uncertainties, in this comparison we adopt a mass range $1 - 100 M_\odot$ for Pop II stars. We checked that for Pop II stars with mass $1 M_\odot$, the fitted main sequence age still agrees with Girardi et al. (2000).

Since Pop II stars are found to contribute much more than Pop III stars to the NIRB (see Figure 3), and stellar emission is the dominant component, we neglect here the nebular emission. L_ν can then be represented by a blackbody spectrum, and we truncate it at $h\nu = 13.6 \text{ eV}$, (Fernandez & Komatsu 2006; Fernandez et al. 2010; Cooray et al. 2012a).

We plot the emissivity at $z = 10$ calculated by different methods in Figure 8 for a star formation efficiency $f_\star = 0.01$ and a minimum mass $M_{\text{min}} = 10^6 M_\odot$. It is not surprising that ‘‘Approximation

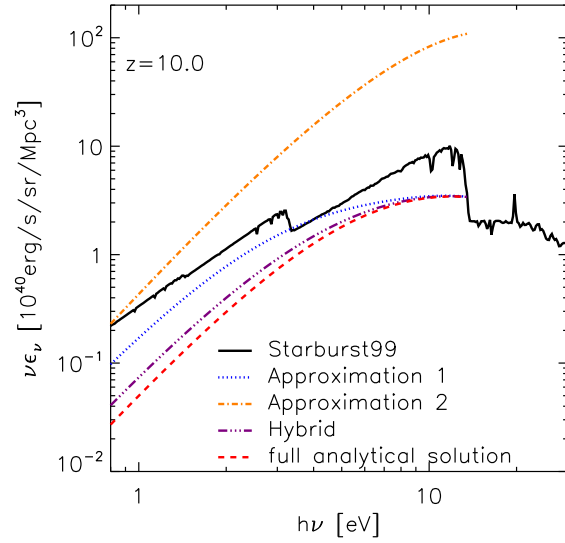


Fig. 8.— Emissivity of Pop II stars at redshift 10.0. The solid line is the result obtained by using the spectrum template from **Starburst99** used here, the dotted line is for the “Approximation 1”; dash-dotted line refers to “Approximation 2”. The dash-dotted-dotted-dotted line corresponds to the “Hybrid” approximation; finally the dashed line refers to the full analytical solution of Eqs (A1-A4) using fitting formulae (see text).

2” overestimates the emissivity, since it assumes that none of the stars die. However, we find that for the stellar mass range $1 - 100 M_{\odot}$, “Approximation 1” also overestimates the emissivity when $h\nu < 8$ eV, because of the contribution of low mass stars whose lifetime is even longer than the age of the universe at that redshift, so that $\tau(m) < t_{\text{SF}}$ is not fulfilled. However, high energy photons come mainly from massive stars, which satisfy $\tau(m) < t_{\text{SF}}$. So at high energies, “Approximation 1” results agree well with the full analytical solution. The “Hybrid” approximation however, is more accurate through the whole range of energy shown in Figure 8; yet, the results still deviate from the full analytical solution.

However, the emissivity calculated from the template of **Starburst99** is still higher than the results obtained from the full analytical solution of Eqs. (A1-A4) with fitting formulae. This is mainly due to the full stellar evolutionary tracks used by **Starburst99**, which extend beyond the zero-age main sequence (ZAMS) stage. For example, the luminosity of a $7 M_{\odot}$ star with metallicity $1/50 Z_{\odot}$ at the end of the main sequence is three times as large as the ZAMS luminosity; at the end of its evolution, the luminosity is $\sim 10\times$ higher compared to ZAMS luminosity. The analogous value for a $100 M_{\odot}$ star of the same metallicity, is about $2\times$ the ZAMS luminosity.